LA-UR- 10-00339

Approved for public release; distribution is unlimited.

Title:	Crystal-field effects in fluoride crystals for optical refrigeration
Author(s):	Markus P. Hehlen
Intended for:	Photonics West 2010 conference San Francisco, CA January 28, 2010

Los Alamos
NATIONAL LABORATORY
EST. 1943

Form 836 (7/06)

Crystal-field effects in fluoride crystals for optical refrigeration

Markus P. Hehlen*
Los Alamos National Laboratory, Mailstop J964, Los Alamos, NM 87545, USA.

1. INTRODUCTION

The field of optical refrigeration of rare-earth-doped solids has recently seen an important breakthrough. The cooling of a $YLiF_4$ (YLF) crystal doped with 5 mol% Yb^{3+} to 155 K by Seletskiy et al [NPhot] has surpassed the lowest temperatures (~170 K for ~100 mW cooling capacity) that are practical with commercial multi-stage thermoelectric coolers (TEC) [Glaister]. This record performance has advanced laser cooling into an application relevant regime and has put first practical optical cryocoolers within reach. The result is also relevant from a material perspective since for the first time, an Yb^{3+}-doped crystal has outperformed an Yb^{3+}-doped glass. For several years, the record temperature of 208 K was held by the Yb^{3+}-doped fluorozirconate glass ZBLAN [Thiede2005]. Advanced purification and glass fabrication methods currently under development are expected to also advance ZBLAN:Yb^{3+} to sub-TEC temperatures [Hehlenbook]. However, the recent achievements with YLF:Yb^{3+} illustrate that crystalline materials may have two potentially game-changing advantages over glassy materials. First, the crystalline environment reduces the inhomogeneous broadening of the Yb^{3+} electronic transitions as compared to a glassy matrix. The respective sharpening of the crystal-field transitions increases the peak absorption cross section at the laser excitation wavelength and allows for more efficient pumping of the Yb^{3+} ions, particularly at low temperatures. Second, many detrimental impurities present in the starting materials tend to be excluded from the crystal during its slow growth process, in contrast to a glass where all impurities present in the starting materials are included in the glass when it is formed by temperature quenching a melt. The ultra high purity required for laser cooling materials [PRB] therefore may be easier to realize in crystals than in glasses.

Laser cooling occurs by laser excitation of a rare-earth ion followed by anti-Stokes luminescence. Each such laser-cooling cycle extracts thermal energy from the solid and carries it away as high-entropy light, thereby cooling the material. In the ideal case, the respective laser-cooling power is given by the pump wavelength (λ_P), the mean fluorescence wavelength ($\bar{\lambda}_L$), and the absorption coefficient (α_r) of the pumped transition. These quantities are solely determined by crystal field interactions. On the one hand, a large crystal-field splitting offers a favorably large difference of $\lambda_P - \bar{\lambda}_L$ and thus a high cooling efficiency $\eta_{cool} = (\lambda_P - \bar{\lambda}_L)/\bar{\lambda}_L$. On the other hand, a small crystal-field splitting offers a high thermal population (n_i) of the initial state of the pumped transition, giving a high pump absorption coefficient and thus high laser cooling power, particularly at low temperatures. A quantitative description of crystal-field interactions is therefore critical to the understanding and optimization of optical refrigeration. In the case of Yb^{3+} as the laser cooling ion, however, the development of a crystal-field model is met with substantial difficulties. First, Yb^{3+} has only two *4f* multiplets, $^2F_{7/2}$ and $^2F_{5/2}$, which lead to at most 7 crystal-field levels. This makes it difficult, and in some cases impossible, to evaluate the crystal-field Hamiltonian, which has at least 4 parameters for any Yb^{3+} point symmety lower than cubic. Second, $^2F_{7/2} \leftrightarrow {}^2F_{5/2}$ transitions exhibit an exceptionally strong electron-phonon coupling compared to *4f* transitions of other rare earths. This makes it difficult to distinguish electronic from vibronic transitions in the absorption and luminescence spectra and to reliably identify the crystal-field levels. Yb^{3+} crystal-field splittings reported in the literature should thus generally be viewed with caution.

This paper explores the effects of crystal-field interactions on the laser cooling performance of Yb^{3+}-doped fluoride crystals. It is shown that the total crystal-field splitting of the $^2F_{7/2}$ and $^2F_{5/2}$ multiplets of Yb^{3+} can be estimated from crystal-field splittings of other rare-earth-doped fluoride crystals. This approach takes advantage of an extensive body of experimental work from which Yb^{3+} doped fluoride crystals with favorable laser cooling properties might be identified. Section 2 reviews the crystal-field splitting of the *4f* electronic states and introduces the crystal-field strength as a means to predict the total crystal-field splitting of the $^2F_{7/2}$ and $^2F_{5/2}$ multiplets. Section 3 illustrates the effect of the total $^2F_{7/2}$ crystal field splitting on the laser cooling power. Finally, Section 4 compiles literature data on crystal-field splittings in fluoride crystals from which the $^2F_{7/2}$ splitting is predicted.

*hehlen@lanl.gov; phone 1 505 665-1737

2. Yb^{3+} IN A CRYSTAL FIELD

This section briefly reviews the origin and properties of the *4f*↔*4f* electronic transitions of Yb^{3+} and introduces the concept of crystal-field strength.

The Yb^{3+} free ion

The electron configuration of the trivalent rare-earth ions is that of the closed xenon shell plus $N = 1..13$ *4f* electrons. The electrostatic interaction between the *4f* electrons causes the $[Xe]4f^N$ configuration to split into several $^{(2S+1)}L$ manifolds. The spin-orbit interaction is of comparable magnitude to the electrostatic interaction for the rare earths, and coupling of $\vec{S}$ and $\vec{L}$ must be considered. It is described by the total angular momentum quantum number $J=|L+S| \ldots |L-S|$. The spin-orbit coupling lifts the degeneracy in $\vec{J}$, thus splitting each $^{(2S+1)}L$ manifold into several $^{(2S+1)}L_{(J)}$ multiplets. The electron configuration of Yb^{3+} is $[Xe]4f^{13}$ and is one electron short of a closed *4f* shell. Therefore it can equivalently be viewed as consisting of the closed xenon and *4f* shells plus one *4f* hole. A single *4f* hole, having a spin of $s=½$ and an angular momentum of $l=3$, creates a total spin of $S=½$ and a total orbital angular momentum $L=3$ and therefore produces a single ^2F manifold which splits into a $^2F_{7/2}$ and a $^2F_{5/2}$ multiplet as a result of the spin-orbit interaction (see Fig. 1). The magnitude of the splitting is given by $E_{LS} = \zeta\left(l + \frac{1}{2}\right)$ [demtroder] with the spin-orbit coupling parameter $\zeta = 2{,}918\ cm^{-1}$ for the Yb^{3+} free ion [Crosswhite1984]. This produces a $^2F_{5/2}$-$^2F_{7/2}$ splitting of ~10,200 cm^{-1} and gives rise to the well-known *4f*↔*4f* electronic transitions of Yb^{3+} at wavelengths around 1 μm..

Crystal-field splitting

There remains degeneracy with respect to J_z in the spherical symmetry of the free ion. In a solid however, the non-spherically symmetric arrangement of charges around the rare-earth ion partially or completely lifts the $(2J+1)$-fold J_z degeneracy and causes each $^{(2S+1)}L_{(J)}$ multiplet to split into several crystal-field levels. According to the Kramers degeneracy theorem, states of odd numbered electron systems in an electric field, such as Yb^{3+} in the crystal field created by the surrounding charges, remain at least doubly degenerate as a result of the time reversal invariance of electric fields. Therefore, the $^2F_{7/2}$ and $^2F_{5/2}$ multiplets split into at most 4 and 3 Kramers doublets, respectively, under the influence of a crystal field (see Fig. 1). A complete lifting of the $(2J+1)$-fold degeneracy with respect to J_z is only possible under the influence of a magnetic field, which is not invariant upon time reversal.

The number of levels into which the $^2F_{7/2}$ and $^2F_{5/2}$ multiplets split under the influence of the crystal field depends on the point symmetry of the electric field produced by the neighboring charges. It can be deduced from group theory by gradually lowering the symmetry from that of the spherical SO_3 symmetry of the free ion down to the C_1 point group of a crystal field with no symmetry. Figure 1 illustrates the qualitative splitting of the $^2F_{7/2}$ and $^2F_{5/2}$ multiplets for various point symmetries as derived using the branching rules by Butler [XX]. Crystal fields of cubic point symmetry (O, O_h, T_d) only partially lift the J_z degeneracy and split the $^2F_{7/2}$ and $^2F_{5/2}$ multiplets into 3 and 2 crystal-field levels, respectively. The J_z degeneracy is completely lifted (except for Kramers degeneracy) for any of the other 29 point symmetries, thus splitting the $^2F_{7/2}$ and $^2F_{5/2}$ multiplets into 4 and 3 crystal-field levels, respectively.

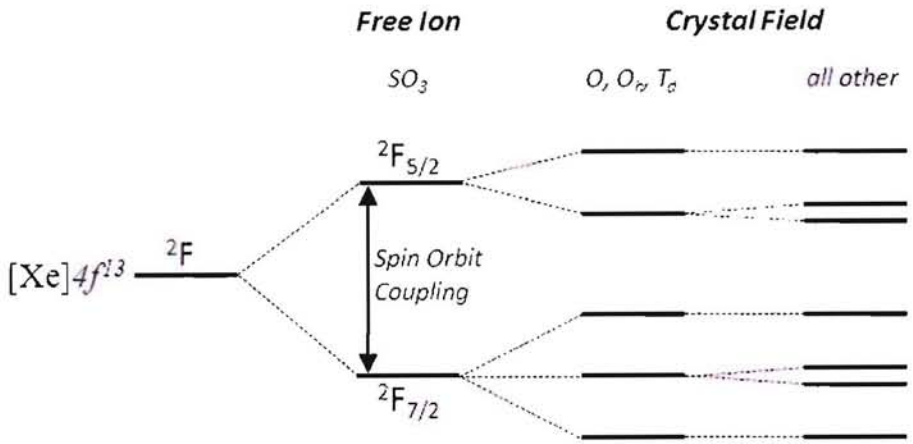

Figure 1. Electronic states of the Yb^{3+} ion. In the free ion, the spin-orbit interaction splits the ^2F manifold into a $^2F_{7/2}$ and a $^2F_{5/2}$ multiplet. The crystal field causes a further splitting into, at most, 4 and 3 Kramers doubly-degenerate crystal-field levels, respectively. Complete lifting of the $(2J+1)$ degeneracy is only achieved in a magnetic field.

Crystal-field strength

The Hamiltonian that quantitatively describes the splitting of $^{(2S+1)}L_{(J)}$ multiplets under the influence of a crystal field is given by

$$\hat{H}_{CF} = \sum_{k,q} B_q^k C_q^k \tag{1}$$

The C_q^k are tensor operators describing the angular dependence of the crystal-field interaction, and they can be evaluated using the techniques outlined in Refs. [XX]. The B_q^k are the crystal-field parameters that capture the radial properties of the crystal field. The number of non-zero B_q^k is limited by $k = 2,4,6$ (for *4f* electron systems) and by the point symmetry of the crystal field [XX]. The B_q^k are difficult to calculate from first principles and are usually obtained by fitting Eq.(1) to a set of experimental crystal-field energies. While excellent crystal-field calculations exist for many rare-earth doped materials, such fitted sets of B_q^k parameters tend to be specific to a rare-earth ion in a specific point symmetry of a specific host crystal.

Auzel et al have suggested the more general description of crystal-field strength in an attempt to identify trends in crystal-field splittings along the series of rare earth ions [Auzel1983, Auzel2002]. They showed that the total splitting $\Delta E(4f^N SLJ)$ of a $^{(2S+1)}L_{(J)}$ multiplet is proportional to the crystal-field strength parameter

$$N_v = \left[\sum_{k,q} \left(B_q^k\right)^2 \left(\frac{4\pi}{2k+1}\right)\right]^{1/2} \tag{2}$$

independent of point symmetry [Auzel1983]. Specifically, the total splitting $\Delta E(4f^N SLJ)$ of a $^{(2S+1)}L_{(J)}$ multiplet is given by

$$\Delta E(4f^N SLJ) = \left[\frac{3g_a^2}{g(g_a+2)(g_a+1)\pi}\right]^{1/2}\left[\prod_{k=2,4,6}\left|\langle J\|C^{(k)}\|J\rangle\right|\right]^{1/3} N_v \tag{3}$$

where $g = 2J + 1$ is the J-degeneracy of the multiplet, and $g_a = g$ and $g_a = g/2$ for even and odd numbered *4f* electron systems, respectively [Auzel1983]. The second term in Eq.(3) contains the reduced matrix elements of $C^{(k)}$, which is the tensor operator for the Coulomb interaction between the *4f* electrons and the electrons of the surrounding charges. Note that the geometric average in the second term assumes the $C^{(k)}$ matrix elements to be of similar magnitude. An analysis of the crystal-field splittings in many compounds has found that N_v decreases linearly along the series of rare earths from Ce^{3+} to Yb^{3+} [Auzel 2002]. Specifically, the crystal-field strength of a $4f^N$ configuration is related to that of the $4f^3$ configuration by [Auzel2002]

$$N_v(4f^N) = N_v(4f^3) - 0.034(N-3)N_v(4f^3) \tag{4}$$

Equations (3) and (4) allow us to estimate the crystal-field splitting of a $^{(2S+1)}L_{(J)}$ multiplet of one $4f^N$ configuration from the crystal-field splitting of a $^{(2S'+1)}L_{(J')}$ multiplet of another $4f^{N'}$ configuration. It should therefore be possible to predict the total crystal-field splitting of the $^2F_{7/2}$ and $^2F_{5/2}$ multiples of Yb^{3+} from crystal-field splittings in other compounds. Auzel et al have used this approach to predict the $^2F_{7/2}$ ground-state splitting of Yb^{3+} from the $^4I_{9/2}$ ground-state splitting of Nd^{3+} [Auzel2002]. In this study we expand on this approach to include all of rare earths in an attempt to best utilize the crystal-field data available in the literature.

Evaluation of the reduced matrix element in Eq.(3) involves tensor operator calculus. The $|\langle J\|C^{(k)}\|J\rangle|$ matrix element is given by

$$\left|\langle J\|C^{(k)}\|J\rangle\right|^2 = \left|\langle l\|C^{(k)}\|l\rangle\right|^2\left|\langle SLJ\|U^{(k)}\|SLJ\rangle\right|^2 \tag{5}$$

The first term in Eq.(5) is given by [Hufner 2.10b]

$$\left|\langle l\|C^{(k)}\|l'\rangle\right| = (-1)^l\sqrt{(2l+1)(2l'+1)}\begin{pmatrix} l & k & l' \\ 0 & 0 & 0\end{pmatrix} \tag{6}$$

where the last factor is a 3*j* symbol. For *4f* electrons ($l = l' = 3$), Eq.(6) evaluates to 1.867, 1.273, and 1.632 for $k = 2,4,6$, respectively. The second term in Eq.(5) further reduces to [Hufner3.7b]

$$\left|\langle SLJ\|U^{(k)}\|SL'J'\rangle\right| = (-1)^{S+L'+J+k}\sqrt{(2J+1)(2J'+1)}\begin{Bmatrix} J & J' & k \\ L' & L & S\end{Bmatrix}\left|\langle SL\|U^{(k)}\|SL'\rangle\right| \tag{7}$$

where the third factor is a 6*j* symbol. The $|\langle SL\|U^{(k)}\|SL'\rangle|$ reduced matrix elements can be calculated from first principles [Nielsen&Koster]. It is important to note, however, that the spin-orbit interaction mixes different states having the same J. As a result, the $^{(2S+1)}L_{(J)}$ multiplets are no longer pure Russel-Saunders wavefunctions but rather a linear

combination $|SLJ\rangle' = \sum_i a_i |S_i L_i J\rangle$, with the coefficients a_i being material specific. In a comprehensive 1978 study, Carnall et al have calculated intermediate coupling wavefunctions $|SLJ\rangle'$ and the respective $\left|\langle SLJ\|U^{(k)}\|SL'J'\rangle\right|^2$ reduced matrix elements for the series of rare-earth-doped LaF_3 [xx]. This crystal is a reasonable approximation for other rare-earth-doped fluoride crystals, and we shall use these reduced matrix elements for the present calculations.

Equation (3) assumes that the variation of $\left|\langle SLJ\|U^{(k)}\|SLJ\rangle\right|^2$ with k is less than 10 and that $J \geq 3$ [Auzel1983]. In addition, there are $^{(2S+1)}L_{(J)}$ multiplets for which one or more of the three $\left|\langle SLJ\|U^{(k)}\|SLJ\rangle\right|^2$ reduced matrix elements ($k = 2,4,6$) is exactly zero by selection rules. These constraints eliminate many multiplets from consideration. Table 1 summarizes an analysis of all $^{(2S+1)}L_{(J)}$ multiplets with energies <30,000 cm^{-1} for the rare earths from Pr^{3+} ($4f^2$) to Tm^{3+} ($4f^{12}$) (Pm^{3+} was excluded for its radioactivity, and Gd^{3+} was excluded for its lack of $4f$ excited states below 30,000 cm^{-1}). We find that 46 multiplets meet the above criteria. Some of these multiplets are energetically close to or overlapping with others (marked by an asterisk), making it difficult to deduce their total crystal-field splitting from absorption spectra. This leaves 35 multiplets that can be considered for analysis with Eq.(3). Table 1 shows in bold the multiples for which reliable crystal-field literature data is available for fluoride crystals. These are the multiplets that will be further analyzed in the following sections.

Table 1. $^{(2S+1)}L_{(J)}$ multiplets of the $4f^2$ through $4f^{12}$ rare-earth ions that have $J \geq 3$ and a variation of the $\left|\langle SLJ\|U^{(k)}\|SLJ\rangle\right|^2$ matrix elements with k of less than 10. Baricenter energies are given in parentheses [Car1978]. Only states with energies below 30,000 cm^{-1} are considered. Pm^{3+} is omitted for its radioactivity, and Gd^{3+} is omitted for its lack of $4f$ excited states with energies below 30,000 cm^{-1}. The matrix elements are those for LaF_3 calculated by Carnall [Carnall1978]. Multiplets for which reliable total crystal-field splitting data in fluoride crystals is available are shown in bold. Multiples marked by an asterisk are energetically close to or overlapping with one or more other multiplets.

Pr^{3+} $4f^2$	Nd^{3+} $4f^3$	Sm^{3+} $4f^5$	Eu^{3+} $4f^6$	Tb^{3+} $4f^8$	Dy^{3+} $4f^9$	Ho^{3+} $4f^{10}$	Er^{3+} $4f^{11}$	Tm^{3+} $4f^{12}$
$^3H_4$ (200)	**$^4I_{9/2}$ (235)**	$^6H_{15/2}$* (6520)	$^7F_3$ (1866)	**$^7F_5$ (2172)**	**$^6H_{15/2}$ (175)**	**$^5I_8$ (0)**	**$^4I_{15/2}$ (219)**	**$^3H_6$ (200)**
$^3H_5$ (2303)	**$^4I_{11/2}$ (2114)**	**$^6F_{7/2}$ (8000)**	$^7F_5$ (3849)	**$^7F_3$ (4423)**	$^6F_{11/2}$* (7853)	**$^5I_7$ (5146)**	**$^4I_{13/2}$ (6701)**	**$^3H_5$ (8336)**
$^3H_6$ (4487)	**$^4I_{13/2}$ (4098)**	**$^6F_{9/2}$ (9200)**	$^5D_3$ (24355)	$^5L_7$* (29595)	$^6F_{9/2}$* (9166)	**$^5I_6$ (8568)**	**$^4I_{11/2}$ (10340)**	**$^3H_4$ (12711)**
	$^4G_{7/2}$ (19293)	$^4I_{11/2}$* (21147)			**$^4H_{15/2}$ (22222)**	**$^5I_5$ (11123)**	**$^4F_{9/2}$ (15453)**	
	$^4G_{9/2}$* (19709)	$^4I_{13/2}$ (21644)			$^4M_{21/2}$ (25109)	**$^5I_4$ (13212)**	**$^4G_{9/2}$ (27635)**	
		$^4M_{21/2}$* (25434)			$^4I_{13/2}$* (25794)	**$^5F_3$ (20596)**	**$^4G_{7/2}$ (28241)**	
					$^4F_{7/2}$* (25856)	**$^3K_8$ (21279)**		
					$^4K_{17/2}$* (25890)	**$^5G_5$ (23942)**		
						$^3H_6$* (27672)		

3. EFFECT OF CRYSTAL FIELD STRENGTH ON LASER COOLING POWER

The laser cooling efficiency of a system that is being pumped at wavelength λ_P and that emits at a mean luminescence wavelength $\bar{\lambda}_L$ is given by [Sheik2007]

$$\eta_{cool} = \eta_{abs}\eta_{ext}\frac{\lambda_P - \bar{\lambda}_L}{\bar{\lambda}_L} \tag{8}$$

The external quantum efficiency $\eta_{ext} = \eta_e\eta_i$ denotes the probability that an excited laser-cooling ion creates a luminescence photon that escapes from the sample. It is determined by the internal quantum efficiency of the luminescent center, η_i, and the photon escape efficiency, η_e. Furthermore, the absorption coefficient at λ_P is $\alpha = \alpha_r + \alpha_b$, where α_r and α_b are the absorption coefficients for resonant absorption by the laser cooling ion and background absorption by impurities, respectively. The absorption efficiency is thus $\eta_{abs} = \alpha_r/(\alpha_r + \alpha_b)$. The product $\eta_{abs}\eta_{ext}$ therefore represents the fraction of absorbed photons that escape the sample as luminescence photons. The laser cooling power then becomes $P_{cool} = P(1 - e^{-\alpha d})\eta_{cool}$, where $P(1 - e^{-\alpha d})$ is the absorbed laser power with P being the incident laser power and d being the optical path length in the sample. In very pure materials, such as the fluoride crystals and glasses being fabricated for laser cooling, parasitic absorption at the pump wavelength by impurities is small, and $\alpha \approx \alpha_r$ in the following. Likewise, the internal quantum efficiency $\eta_i \approx 1$ in a very pure material. Finally, light trapping is inefficient in fluoride materials due to their relatively low index of refraction, i.e. $\eta_e \approx 1$. Therefore we shall assume $\eta_{abs}\eta_{ext} = 1$ in the following. The laser cooling power is then solely determined by $\bar{\lambda}_L$, λ_P, and α_r. Here, $\alpha_r = n_i\sigma_r N$, where n_i is the thermal population of the initial state of the pumped transition, σ_r is the pump absorption cross section, and N is the ion density. These quantities are largely determined by the $^{(2S+1)}L_{(J)}$ multiplet energies and the crystal-field interactions.

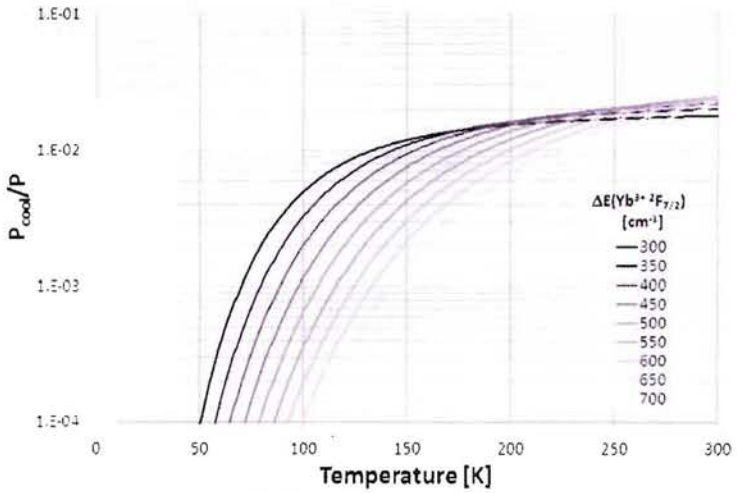

Figure 2. Calculated cooling efficiency as a function of temperature for different total crystal-field splittings of the $^2F_{7/2}$ ground-state multiplet of Yb^{3+}. Refer to text for model assumptions.

Let us assume an Yb^{3+} ion in a cubic crystal field, which produces a splitting of the $^2F_{7/2}$ and $^2F_{5/2}$ multiplets in 3 and 2 crystal-field levels, respectively (see Fig. 1). The total crystal-field splittings of these multiples are related by Eq.(3). We find that $\Delta E\left(4f^{13}\,^2F_{5/2}\right) = 0.74 \cdot \Delta E\left(4f^{13}\,^2F_{7/2}\right)$ in cubic symmetry, where the crystal-field interaction is limited to terms with $k = 4$ and $k = 6$. We further assume a fixed spin-orbit splitting of 10,200 cm^{-1} of the $^2F_{7/2}$ and $^2F_{5/2}$ baricenters and all 6 crystal-field transitions to have the same cross section of α_r=10^{-21} cm^2 [Weber1983]. The ion density is assumed to be 1.2×10^{21} cm^{-3}, such as in YLF:10%Yb^{3+}, and the optical path length is taken as 15 round-trips through a 1 cm long sample, i.e. d=30 cm. λ_P is given by the energy of the pumped $^2F_{7/2}(2)\rightarrow{}^2F_{5/2}(0')$ transition, and $\bar{\lambda}_L$

is given by the energies of the various $^2F_{5/2}(j) \rightarrow {}^2F_{5/2}(i)$ emission transitions weighed by the thermal population n_j of the respective initial state.

Figure 2 shows the cooling efficiency as a function of temperature for different $^2F_{7/2}$ total crystal-field splittings calculated from the simple model described above. While a decreasing crystal-field splitting reduces the cooling efficiency at room temperature via the term $(\lambda_P - \bar{\lambda}_L)/\bar{\lambda}_L$, this decrease is outweighed at cryogenic temperatures by a significant increase in the initial-state thermal population of the pumped transition, n_i. The initial state population becomes the dominant factor determining the cooling efficiency at low temperatures. At 100 K for example, a system with a 300 cm^{-1} $^2F_{7/2}$ splitting cools four times as efficient as a system with a 450 cm^{-1} $^2F_{7/2}$ splitting. Laser cooling at cryogenic temperatures with reasonable efficiencies is thus only possible with materials having a small crystal-field splitting of the ground-state multiplet.

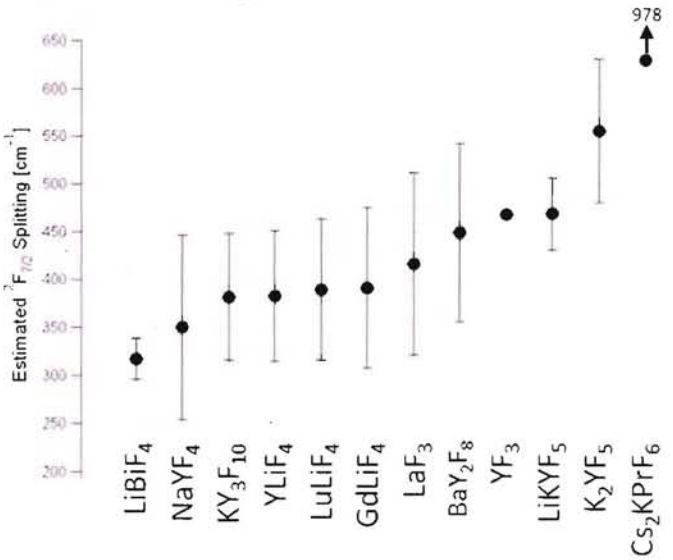

Figure 3. Average total crystal-field splitting of the $^2F_{7/2}$ multiplet of Yb^{3+} in fluoride crystals as estimated from Eqs. (3) and (4) and compiled from Table 2.

4. TRENDS IN Yb^{3+} CRYSTAL-FIELD SPLITTING IN FLUORIDE CRYSTALS

Determination of the crystal-field energies of a rare-earth-doped crystal is quite laborious. It involves growing the crystal and measuring absorption and luminescence spectra at different temperatures. In the case of Yb^{3+} there is the additional complication of relatively strong electron-phonon coupling, which makes unambiguous interpretation of the spectra difficult in most cases. In this section we attempt to estimate the crystal-field splitting of Yb^{3+} doped fluoride crystals from crystal-field data from other rare-earth-doped fluoride crystals that are available in the literature. The goal is to identify crystals with a small $^2F_{7/2}$ splitting suited for laser cooling. Our comprehensive survey of the literature has found 25 publications on 12 different fluoride crystals that provide reliable crystal-field splitting data for the $^{(2S+1)}L_{(J)}$ multiplets listed in Table 1. These splittings are shown in Table 2 along with the $^2F_{7/2}$ splitting estimated from Eqs. (3) and (4) (see Section 2). Figure 3 summarizes the findings and shows the average estimated $^2F_{7/2}$ crystal-field splitting for the various crystals.

Table 2. Total crystal-field splitting ΔE of $^{(2S+1)}L_{(J)}$ multiplets in fluoride crystals from the literature. The multiplets listed here meet the conditions of Table 1. The last column gives the predicted splitting of the $^2F_{7/2}$ ground-state multiplet of Yb^{3+} as calculated from Eqs.(3) and (4) along with the average and standard deviation for each crystal.

Host (Symmetry)	Ion	$^{(2S+1)}L_{(J)}$	ΔE	Ref	$\Delta E(^2F_{7/2})$
$LiBiF_4$	Pr	$^3H_4$	501	[#21]	331
(S_4)	Pr	$^3H_5$	357	[#21]	293
	Pr	$^3H_6$	601	[#21]	328
					317±21
$NaYF_4$	Nd	$^4I_{9/2}$	443	[#19]	488
(C_{3h})	Nd	$^4I_{11/2}$	173	[#19]	311
	Nd	$^4I_{13/2}$	270	[#19]	372
	Nd	$^4I_{9/2}$	384	[#19]	423
	Nd	$^4I_{11/2}$	128	[#19]	230
	Nd	$^4I_{13/2}$	199	[#19]	274
					350±96
KY_3F_{10}	Pr	$^3H_4$	508	[#13]	336
(C_{4v})	Pr	$^3H_5$	450	[#13]	369
	Pr	$^3H_6$	682	[#13]	372
	Ho	$^5I_8$	292	[#14]	337
	Ho	$^5I_7$	191	[#14]	496
					382±66
$YLiF_4$	Pr	$^3H_4$	514	[#21]	340
(S_4)	Pr	$^3H_5$	357	[#21]	293
	Pr	$^3H_6$	636	[#21]	347
	Nd	$^4I_{9/2}$	523	[#22]	576
	Nd	$^4I_{11/2}$	222	[#22]	399
	Nd	$^4I_{13/2}$	308	[#22]	424
	Sm	$^6F_{7/2}$	90	[#23]	436
	Sm	$^6F_{9/2}$	94	[#23]	342
	Ho	$^5I_8$	314	[#9]	362
	Ho	$^5I_7$	141	[#9]	366
	Ho	$^5I_6$	126	[#9]	331
	Ho	$^5I_5$	95	[#9]	309
	Ho	$^5I_4$	351	[#9]	506
	Ho	$^5F_3$	128	[#9]	357
	Er	$^4I_{15/2}$	355	[#24]	409
	Er	$^4I_{13/2}$	205	[#24]	387
	Er	$^4I_{11/2}$	114	[#24]	432
	Er	$^4F_{9/2}$	162	[#24]	425
	Tm	$^3H_6$	419	[#25]	343
	Tm	$^3H_5$	251	[#25]	307
	Tm	$^3H_4$	292	[#25]	359
					383±68

Host (Symmetry)	Ion	$^{(2S+1)}L_{(J)}$	ΔE	Ref	$\Delta E(^2F_{7/2})$
$LuLiF_4$	Ho	$^5I_8$	332	[#9]	383
(S_4)	Ho	$^5I_7$	147	[#9]	381
	Ho	$^5I_6$	132	[#9]	347
	Ho	$^5I_5$	99	[#9]	322
	Ho	$^5I_4$	369	[#9]	532
	Ho	$^5F_3$	132	[#9]	368
					389±74
$GdLiF_4$	Nd	$^4I_{9/2}$	496	[#8]	546
(S_4)	Nd	$^4I_{11/2}$	254	[#8]	456
	Nd	$^4I_{13/2}$	278	[#8]	383
	Ho	$^5I_8$	304	[#9]	351
	Ho	$^5I_7$	134	[#9]	348
	Ho	$^5I_6$	120	[#9]	315
	Ho	$^5I_5$	90	[#9]	293
	Ho	$^5I_4$	331	[#9]	477
	Ho	$^5F_3$	124	[#9]	346
					391±84
LaF_3	Pr	$^3H_4$	508	[#15]	336
(C_{2v})	Nd	$^4I_{9/2}$	500	[#16]	550
	Nd	$^4I_{11/2}$	245	[#16]	440
	Nd	$^4I_{13/2}$	360	[#16]	496
	Nd	$^4G_{7/2}$	177	[#16]	348
	Sm	$^6F_{7/2}$	100	[#16]	484
	Sm	$^6F_{9/2}$	98	[#16]	356
	Dy	$^6H_{15/2}$	335	[#16]	312
	Dy	$^4H_{15/2}$	357	[#16]	402
	Ho	$^5I_8$	412	[#17]	475
	Ho	$^5I_7$	119	[#17]	309
	Ho	$^5I_6$	115	[#17]	302
	Ho	$^5I_5$	82	[#17]	267
	Ho	$^5F_3$	122	[#17]	341
	Ho	$^3K_8$	168	[#17]	523
	Ho	$^5G_5$	135	[#17]	465
	Er	$^4I_{15/2}$	443	[#16]	511
	Er	$^4I_{13/2}$	219	[#16]	414
	Er	$^4I_{11/2}$	94	[#16]	356
	Er	$^4F_{9/2}$	136	[#16]	357
	Er	$^4G_{9/2}$	65	[#16]	625
	Er	$^4G_{7/2}$	31	[#16]	488
					416±95

(Table 2 continued)

Host (Symmetry)	Ion	$^{(2S+1)}L_{(J)}$	ΔE	Ref	$\Delta E(^2F_{7/2})$
BaY_2F_5	Nd	$^4I_{9/2}$	546	[#1]	601
(C_2)	Nd	$^4I_{11/2}$	305	[#1]	548
	Nd	$^4I_{13/2}$	352	[#1]	485
	Nd	$^4G_{7/2}$	186	[#1]	365
	Tb	$^7F_5$	204	[#2]	239
	Tb	$^7F_3$	96	[#2]	300
	Dy	$^6H_{15/2}$	585	[#3]	545
	Ho	$^5I_6$	178	[#4]	468
	Ho	$^5F_3$	164	[#4]	458
	Er	$^4I_{13/2}$	249	[#5]	471
	Er	$^4I_{11/2}$	121	[#5]	458
	Er	$^4F_{9/2}$	187	[#5]	491
	Tm	$^3H_6$	515	[#6]	421
	Tm	$^3H_5$	350	[#6]	428
	Tm	$^3H_4$	366	[#6]	450
					449±93
YF_3	Dy	$^6H_{15/2}$	502	[#20]	467
					467

Host (Symmetry)	Ion	$^{(2S+1)}L_{(J)}$	ΔE	Ref	$\Delta E(^2F_{7/2})$
$LiKYF_5$	Er	$^4I_{15/2}$	380	[#18]	438
(C_1)	Er	$^4I_{13/2}$	264	[#18]	499
	Er	$^4F_{9/2}$	196	[#18]	514
	Er	$^4I_{15/2}$	360	[#18]	415
	Er	$^4I_{13/2}$	246	[#18]	465
	Er	$^4F_{9/2}$	182	[#18]	477
					468±37
K_2YF_5	Pr	$^3H_4$	741	[#10]	490
(C_{2v})	Pr	$^3H_5$	576	[#10]	472
	Pr	$^3H_6$	821	[#10]	448
	Nd	$^4I_{9/2}$	555	[#11]	611
	Nd	$^4I_{11/2}$	381	[#11]	685
	Nd	$^4I_{13/2}$	422	[#11]	581
	Nd	$^4G_{7/2}$	280	[#11]	550
	Tm	$^3H_6$	704	[#12]	576
	Tm	$^3H_4$	475	[#12]	584
					555±75
Cs_2KPrF_6*	Pr	$^3H_4$	1241	[#7]	978
(O_h)					***978***

The formalism of Section 2 correctly predicts the $^2F_{7/2}$ crystal-field splittings that are typical for fluoride systems, with most crystals falling in the 350-450 cm^{-1} range. It is evident from Figure 3, however, that the predicted crystal-field splittings have a rather substantial standard deviation of ±18% on average. Such a large error prevents us from revealing more subtle trends within the family of fluoride crystals and from identifying specific crystals suited for laser cooling. $YLiF_4$, the crystal that recently achieved laser cooling to a new record low temperature [XX], is among the group of several crystals with a low splitting around 380 cm^{-1}. Only KY_3F_{10}, $NaYF_4$, and $LiBiF_4$ are predicted to have a smaller $^2F_{7/2}$ crystal-field splitting than $YLiF_4$. $NaYF_4$ can be excluded as it does not form large bulk crystals. The low predicted $^2F_{7/2}$ splitting of 317±21 cm^{-1} of $LiBiF_4$ warrants further study. While XSchultheissXX has noted difficulties in growing $LiBiF_4$ crystals [xx], this compound is a possible candidate for laser cooling. $LiKYF_5$, K_2YF_5, and Cs_2KLnF_6 fall on the high end of the predicted $^2F_{7/2}$ splittings and do not favor efficient laser cooling at cryogenic temperatures.

5. CONCLUSIONS

The concept of crystal-field strength was used to predict the $^2F_{7/2}$ ground-state splitting of Yb^{3+} in fluoride crystals based on crystal-field data fluoride crystals doped with other rare-earth ions. The formalism correctly predicts the $^2F_{7/2}$ splitting of 350-450 cm^{-1} typical of these materials. The formalism also predicts the $^2F_{7/2}$ crystal-field splitting in $LiKYF_5$, K_2YF_5, and Cs_2KLnF_6 to be >450 cm^{-1}, which is unfavorably large for laser cooling. The crystal-field strength formalism however fails to provide the accuracy needed to reveal the more subtle trends within the group of crystals with a small $^2F_{7/2}$ splitting. The current record laser-cooling material YLF:Yb^{3+} falls in this group. For the crystals studied here, the lowest $^2F_{7/2}$ splitting is predicted for $LiBiF_4$.

ACKNOWLEDGMENTS

I gratefully acknowledge the fruitful discussions with F. Auzel on the formalism discussed in Section 2 and with R.I. Epstein.

REFERENCES